ISSN:2790-1688 Volume-15-(2025)

Research on fragment dispersion characteristics of focused warhead with eccentric initiation

Mingze Li [1], Peizhuo Shi [1], Wang Yao [1], Shuangxing Liu [1], Junxian Li [1], and Yongxiang Dong [1]

[1] State Key Laboratory of Explosion Science and Safety Protection, Beijing Institute of Technology; Beijing 100081, P. R. China

Abstract. To enhance the damage effectiveness of focused warheads against targets, the research investigates the effects of the number and positions of eccentric initiation points on fragment dispersion characteristics in focused warheads. First, the numerical simulation was verified via central initiation experiment for focused warheads. Based on the verified numerical model, fragment dispersion with different initiations was further simulated. The results reveal main effects on the velocity gain zone, average fragment velocity, average kinetic energy, energy density, effective fragment count, and dispersion angle, which exhibit regular variations with changes in the number and positions of initiation points. Specifically, under the research conditions of the work, as the number of axial initiation points increases, the velocity gain zone expands. In contrast, the warhead dispersion angle, fragment velocity, and kinetic energy peak and then decline, while the energy density initially decreases and then exhibits slight fluctuations. The findings could be a reference for optimizing charge initiation design and improving the damage effect of focused warheads.

Keywords: Focused warhead; Eccentric initiation; Dispersion characteristics; Influence laws.

1. Introduction

Modern battlefield operations are becoming increasingly diversified and composite, with targets featuring higher speed, enhanced maneuverability, and improved protection[1]. To enhance strike effectiveness, focused fragmentation warheads construct a high-density fragment zone (focusing fragment zone) by controlling fragment distribution within a small dispersion angle, which can effectively improve damage capability[2]. Traditional central initiated warheads exhibit axisymmetric dispersion of fragments. In contrast, eccentric initiated warheads control the detonation wave propagation by using the offsetting of initiation points to enhance the fragment velocity in the aiming direction (opposite direction of the initiators). When the target occupation azimuths coincide with the aiming zone, the best damage can be achieved[3]. To obtain as many effective fragments as possible and improve killing performance, warheads often use pre-controlled fragments and prefabricated fragments[4]. For prefabricated fragment warheads, fragments are pre-processed and shaped, and the expansion radius of the fragment layer is small, so the initial velocity of prefabricated fragments is approximately 10%–20% lower than that of natural fragments. Compared with prefabricated fragments, pre-controlled fragmentation technology can control or guide the casing to fragment as required. It not only controls the size and shape of fragments but also appropriately extends the duration of explosive action on the casing. Grooving the casing is a common method for pre-controlled fragmentation. Moreover, compared with fully prefabricated block or spherical fragments, using grooved casings to form fragments not only simplifies the loading process but also maximizes the use of the projectile space and increases the mass of individual fragments [5]. Currently, scholars worldwide have conducted extensive research on the power field of prefabricated directional warheads. Li et al. [6] researched the mechanism of velocity enhancement of asymmetrically two-line initiated warhead and proposed a new formula of computing the fragment velocity in the aiming direction. Guo et al. [7] analyzed the effects of eccentric initiation and shell strength on the fragment dispersion characteristics of casing. Chen [8] constructed an initiation control model based on hexagon-detection fuze and researched the fragment dispersion law in the directional zone under six-point initiation. Rong et al. [9] analyzed the influence of the number and position of initiation points on the fragment dispersion

characteristics of double-focused warheads. From the above analysis, it can be seen that eccentric focused warheads exhibit different characteristics from central initiation in terms of fragment velocity, quantity, and spatial distribution, and can concentrate damage energy toward the target, enhancing target damage efficiency. However, current research on the fragment dispersion characteristics of eccentrically initiated semi-prefabricated focused warheads still needs to be further deepened. Therefore, this research takes the stacked ring groove semi-prefabricated focused warhead as the research object, mainly investigating the influence of the number of eccentric initiation points, their axial positions, and circumferential angles on fragment velocity, direction, and energy. It also analyzes the optimal eccentric initiation mode for semi-prefabricated focused warheads and researches the gain of relevant indicators compared with central initiation.

2. Verification of Numerical Simulation

2.1 Simulation Model Establishment

To validate the accuracy of numerical simulations in calculating fragment size, velocity, and energy distribution while ensuring the model faithfully replicates physical phenomena observed in experiments, feasibility verification of the numerical simulation was conducted. A focused warhead with a casing featuring a stacked ring groove structure was selected for central initiation experiment to ensure consistent fragment shape and size. An identical finite element model matching the experimental configuration was established for simulation feasibility verification.

To evaluate the damage performance of fragments, this research focused on analyzing fragment dispersion characteristics. Considering computational efficiency and accuracy requirements, the Lagrange algorithm was applied to simulate the dynamic behavior of the casing under detonation-driven loading, while the Smoothed Particle Hydrodynamics (SPH) method was used to model the detonation process of the explosive charge.

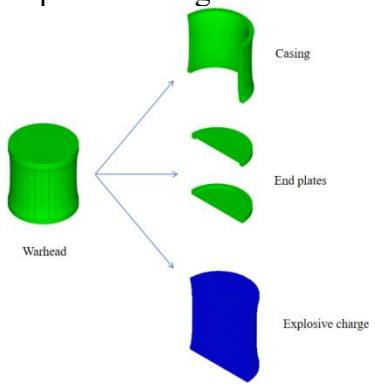

Fig. 1 Three-dimensional simulation model of the warhead

The established three-dimensional simulation model and its overall axonometric view are shown in Fig. 1. The semi-preformed casing adopts axially arranged stacked rings identical to the experimental model. Each ring features uniformly distributed circumferential grooves, facilitating casing fracture along these weakened grooves under detonation-driven loading to form relatively uniform fragments. The main parameters are shown in Table 1.

Table 1 Main structural parameters of the warhead

Explosive charge length L/mm	190.0
Maximum explosive charge radius r_2/mm	86.0
End cap thickness d/mm	8.0
Casing thickness δ/mm	12.0
Circumferential groove depth a/mm	10.8
Circumferential groove count n	30.0

The simulation model consists of three parts, namely the semi-preformed casing, explosive charge and end plates. The casing and end plates are made of 40Cr steel, which offers high tensile strength, excellent impact toughness, and favorable mechanical properties; the explosive charge is made of Composition B, primarily composed of RDX and TNT. This formulation exhibits high detonation velocity with relatively low sensitivity, making it widely adopted in engineering applications. The following description briefly introduces the fundamental equations governing these materials and their main parameters.

2.1.1 Material model of casing

The Johnson-Cook constitutive equation [10] is widely used in explosive impact problems, which typically involve high strain-rate effects. This model accounts for plastic strain, strain rate, and temperature effects under high-strain-rate conditions. Specifically, it decouples these three variables and employs a multiplicative relationship to characterize their combined influence on dynamic yield stress. Consequently, it can effectively describe the mechanical response of metal casings subjected to detonation-driven loading. The yield stress is expressed as:

$$\sigma_{\mathrm{Y}} = \left(A + B\bar{\varepsilon}_{\mathrm{p}}^{n}\right)\left(1 + C\ln\dot{\varepsilon}^{*}\right)\left(1 - T_{\mathrm{H}}^{m}\right) \tag{1}$$

where A, B, and n represent the initial yield stress at reference strain rate and temperature, strain hardening modulus, and hardening exponent, respectively; C denotes the strain rate sensitivity coefficient; $\bar{\varepsilon}_{\mathrm{p}}$ signifies effective plastic strain; and m is the thermal softening parameter.

The main parameters for the 40Cr steel casing material are listed in Table 2.

Table 2 Main parameters of 40Cr steel

ρ/(g/cm^3)	A/(GPa)	B/(GPa)	C	n	m	T_m/(K)
7.8	905	226	0.03	0.2	0.8	1793

2.1.2 Material model of explosive charge

The JWL equation of state [11] is commonly used to describe the detonation process of high-energy explosives. This process involves highly energetic chemical reactions, in which solid explosives rapidly transform into high-temperature, high-pressure detonation products and release substantial energy within an extremely short duration. The equation is commonly adopted in numerical simulations to describe the process:

$$P = A\left(1 - \frac{\omega}{R_1 V}\right)\mathrm{e}^{-R_1 V} + B\left(1 - \frac{\omega}{R_2 V}\right)\mathrm{e}^{-R_2 V} + \frac{\omega E}{V} \tag{2}$$

where P denotes the pressure of detonation products; E represents internal energy per unit volume; V is the relative volume; and A, B, R1, R2, ω are constants typically determined through cylinder tests of explosives.

The main parameters for the explosive charge material Composition B are listed in Table 3.

Table 3 Main parameters of Composition B

/(g/cm^3)	D/(m/s)	P_{CJ}/(GPa)	A/(GPa)	B/(GPa)	R_1	R_2	ω
1.7	7980	29.5	524.2	7.7	4.2	1.1	0.3

2.2 Simulation Model Verification

The experimental site layout is shown in Fig. 2. A steel target plate was positioned 4 m from the warhead for fragment recovery. The measured width of the 90% fragment dispersion zone was 0.51 m, as illustrated in Fig. 3. Numerical simulations yielded a focusing band width of 0.54 m for 90% fragments at 4 m from the initiation center, showing an error of 5.9% from experimental results (Fig.

4). Recovered experimental fragments demonstrate high consistency with simulated fragments in both shape and size, as evidenced in Fig. 5.

Fig. 2 Experimental layout

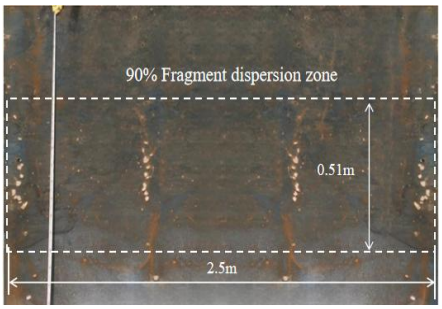

Fig. 3 Perforation pattern on witness plate

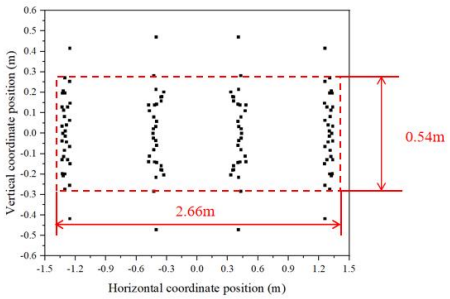

Fig. 4 Perforation pattern on virtual target plate

Fig. 5 Comparison between simulated and experimental recovered fragments

The theoretical fragment velocity can be calculated using the Gurney formula as shown below：

$$v = \sqrt{2E}\sqrt{\frac{\beta}{1+0.5\beta}} \tag{3}$$

where the loading ratio β represents the mass ratio of explosive and casing. Since the Gurney formula typically computes velocities for naturally fragmented casings, semi-preformed casings experience significantly shorter expansion durations and initiate fracture earlier to form fragments. Therefore, 85% of the Gurney-calculated velocity is adopted as the theoretical velocity for semi-preformed fragments, yielding 1458.9 m/s. Measured from the explosive's top surface, the axial fragment position normalized by explosive length is denoted x/L. Simulation results indicate that fragment velocity initially increases then decreases with axial position (Fig. 6). The average velocity is 1409.6 m/s, showing an error of 3.4% from the theoretical value, confirming good agreement between simulation and theoretical predictions.

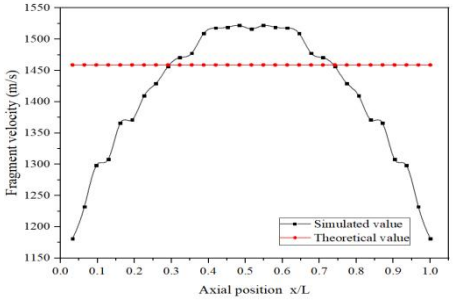

Fig. 6 Simulated and theoretical values of fragment velocity for the focused warhead

In summary, the simulation results are in good agreement with experimental results regarding fragment size, mass, and axial dispersion characteristics, validating the rationality of the selected models and the accuracy of the detonation-driven fragment dispersion mechanism simulation. Building upon the experimental verification of simulation feasibility for a focused warhead with fragment mass of approximately 9 g, and considering the significant advantages of low-mass fragments in enhancing lethality density at extended ranges—as noted by Carlucci et al. [12], small fragments exhibit superior velocity retention capabilities, maintaining higher velocities at longer distances while causing greater permanent tissue damage through tumbling or yawing upon impact; Zhang et al. [13] experimentally confirmed that low-mass fragments outperform medium/heavy fragments in concrete fragmentation effectiveness, making them ideal for field fortification strikes—this research subsequently focuses on warheads with fragment mass of approximately 4 g. The circumferential groove count in the casing was increased to 60 while maintaining other parameters. With single-point central initiation as the control case, the effects of various eccentric initiation modes on fragment dispersion characteristics at 12 m from the warhead center are investigated.

3. Effects of Eccentric Initiation on Fragment Focused Warhead

3.1 Analysis on Multi-Point Eccentric Symmetrical Initiation

When employing multi-point eccentric initiation in warheads, initiation points can be distributed along one or multiple lines. Significant velocity gain is typically achieved with initiation points distributed along two lines, while simultaneously reducing explosive mass loss caused by initiation devices. Therefore, this research sets the number of initiation points n as an even integer, uniformly distributed along two explosive generatrices symmetrical about the explosive axis. Each generatrix contains n/2 initiation points, with corresponding points on both generatrices sharing identical axial coordinates and positioned within planes parallel to the equatorial plane.

When the number of eccentric initiation points n=2, two spherical detonation waves of equal intensity propagate outward from each initiation point upon explosive detonation. When the collision angle reaches a certain value, Mach reflection occurs, as shown in Fig. 7. According to Reference [14], the pressure generated by Mach reflection in Composition B is approximately 2-3 times the CJ pressure, concentrating substantial energy locally on the casing and thereby effectively increasing fragment velocity in the directional zone.

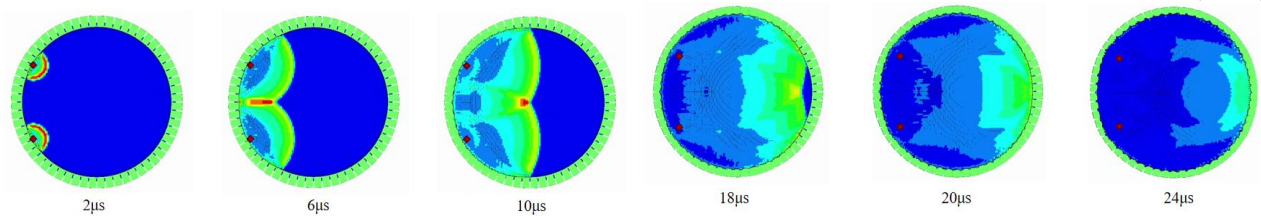

Fig. 7 Detonation-driven process at characteristic time instants under two-point eccentric initiation

When the number of initiation points n>2, the detonation waves of adjacent initiation points collide to form multiple Mach waves, which continue propagating and colliding before acting on the fragments in the directional zone, driving the fragments to achieve higher flying velocities.

3.2 Effects of Number of Initiation Points on Fragment Focused Warhead

With multi-point eccentric initiation, increasing the number of points leverages detonation wave superposition to influence explosive loading characteristics on the casing. However, higher quantities impose greater design challenges for initiation structures. Therefore, rational design of initiation points holds significant theoretical and practical importance for eccentrically initiated focused warheads.

A semi-preformed focused warhead model with multi-point eccentric symmetrical initiation was established, with initiation point quantities n=2,4,6,8. Eccentric initiation points were symmetrically distributed along two curved generatrices of explosive with an included angle of 60°. Each generatrix contained n/2 initiation points at equally spaced angular positions. A top-view of initiation points arrangement is shown in Fig. 8, while corresponding axial cross-sections for each initiation mode are presented in Fig. 9.

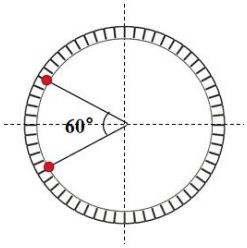

Fig. 8 Top-view schematic of initiation point positions

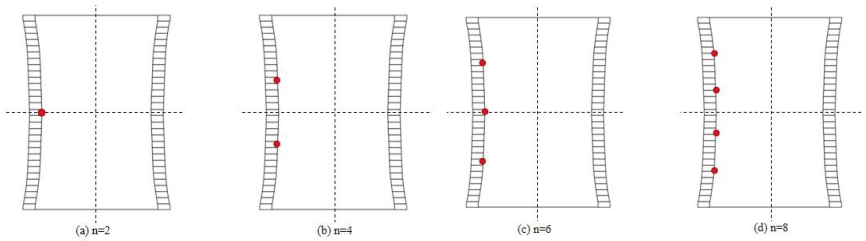

Fig. 9 Axial schematic of initiation point positions

The dispersion angle serves as a critical indicator for evaluating warhead strike efficiency against targets. It is defined as the conical angle with the warhead center as its vertex in the axial plane, encompassing 90% of fragments. This angle is determined by fragment dispersion directions. Based on previous researches, Shapiro proposed the following calculation formula for dispersion direction:

$$\delta = \frac{v_0}{2D}\sin\alpha_c \tag{4}$$

where D denotes explosive detonation velocity, v0 represents casing expansion velocity, and α_c signifies the angle between the detonation wave front and casing wall surface.

With the symmetry line of initiation points as the reference, the aiming direction is denoted as θ=0° and the initiation side as θ=180°. Fragment velocity distributions along the circumferential direction were statistically analyzed. To facilitate quantitative comparison, regions in the aiming direction exceeding 15% of the maximum central initiation velocity are defined as velocity gain zone. Fragments within velocity gain zone that fall within the axial 90% range relative to the warhead geometric center are identified as effective fragments. Based on extracted simulation data, the coverage of velocity gain zone, the number of effective fragments within these regions, distribution density of effective fragments, and warhead dispersion angle at 12 m from the explosive center in the velocity gain zone direction were calculated, as shown in Table 4.

Table 4 Statistical data of fragment velocity gain zone

Number of initiation points *n*	Velocity gain zone coverage	Velocity gain zone angle /°	The number of effective fragments in gain zone /units	Dispersion angle /°	Fragment distribution density (units/m^2)
2	[156°,204°]	48	228	3.4	34.2
4	[138°,222°]	84	394	5.4	17.4
6	[138°,222°]	84	394	5.0	19.0
8	[132°,228°]	96	448	5.1	17.1

The data in Table 4 indicates that increasing the number of initiation points enhances explosive energy release, resulting in more high-velocity fragments circumferentially and expanded velocity gain zone. When the number of initiation points increases from 2 to 4, the velocity gain zone and effective fragments within the gain zone increase by 36° (75%) and 166 units (72.8%) respectively. When further increasing from 4 to 8 points, these parameters increase by 12° (14.2%) and 54 units (13.7%) respectively. Velocity vector of fragments at 100 μs post-initiation is shown in Fig. 10. Increasing initiation points from 2 to 4 shifts axial positions closer to the explosive ends, allowing earlier axial sparse wave propagation into the explosive. This causes end fragments to deviate more from the horizontal plane, increasing the warhead dispersion angle by 2° (58.8%). For conditions with n=4, 6, and 8 initiation points, dispersion angles at 12 m from the explosive center do not change significantly with a maximum variation of 0.4°. Effective fragment density correlates with both velocity gain zone angle and dispersion angle. Maximum density occurs at n=2, while minimum density at n=8, with a difference of 17.1 units/m² (50%).

At 100 μs post-initiation, fragment velocities stabilize. A planar virtual target plate is established with its origin positioned 12 m from the warhead center along the 180° direction and at equivalent height to the warhead center. Fragment coordinates on the virtual plate are calculated by extracting velocities of all fragments within the velocity gain zone at 100 μs. The resulting fragment distribution are shown in Fig. 11. Numerical analysis shows that at n=2, fragments within the velocity gain zone exhibit the most concentrated axial distribution but with lower quantity. For n=4, 6, and 8, fragment quantities increase while maintaining relatively concentrated axial distributions.

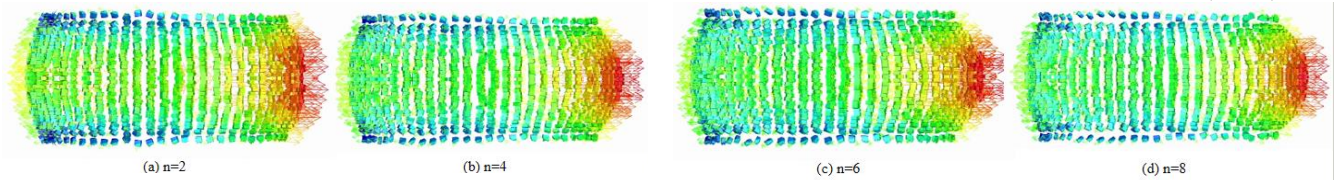

Fig. 10 Fragment velocity vector at 100 μs post-initiation for all initiation modes

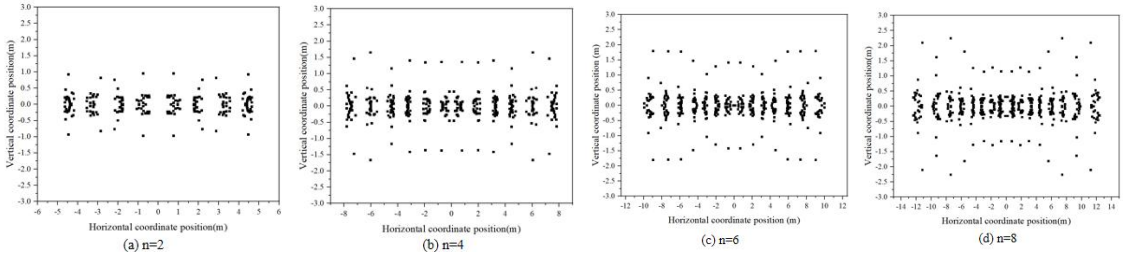

Fig. 11 Fragment distribution on virtual target plate at 12 m for velocity gain zone

By post-processing, the distribution of maximum fragment velocities per circumferential column within the $\theta \in [132^{\circ}, 228^{\circ}]$ angular sector of the velocity gain zone is shown in Fig. 12. As the number of initiation points increases, maximum fragment velocities in the velocity gain zone gradually rise. For all initiation modes, the velocity profile remains consistent, with peak velocities occurring at θ=180° and decreasing gradually toward both sides.

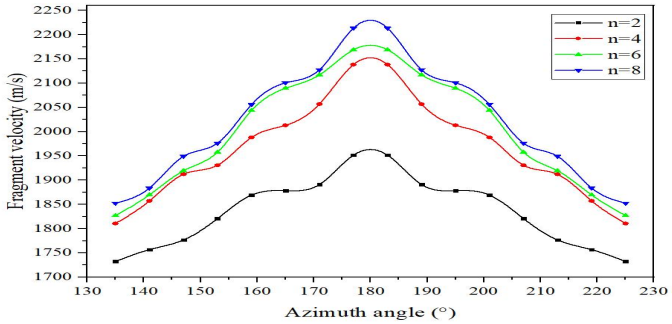

Fig. 12 Fragment velocity distribution within the velocity gain zone

Fragment energy acting on targets and its distribution density serve as common indicators for evaluating warhead lethality, including fragment kinetic energy, specific kinetic energy, and energy density. Energy density, defined as the areal energy density of fragment cloud, characterizes the warhead's regional damage capability. Table 5 summarizes the velocity, kinetic energy, and specific kinetic energy of effective fragments within the velocity gain zone for all initiation modes. Energy density at 12 m from the explosive center was calculated based on effective fragment distribution density and average kinetic energy.

Table 5 Fragment velocity and energy in velocity gain zone

Number of initiation points *n*	2	4	6	8
Maximum velocity (m/s)	1951.6	2138.3	2169.0	2213.6
Average velocity (m/s)	1814.7	1846.7	1880.7	1867.5
Average kinetic energy (J)	7310.9	7570.6	7852.0	7742.4
Average specific kinetic energy (J/cm^2)	14059.4	14558.8	15100.1	14889.3
Energy density (J/m^2)	249966.6	131484.1	149387.1	132189.7

The above data indicates that with fewer initiation points, Mach reflection is incomplete, generating Mach overpressure only near the initiation points and failing to fully utilize explosive energy. As the number of initiation points n increases, the superposition effect of detonation waves enhances shock wave damage efficacy, progressively increasing fragment velocity and kinetic

energy within the velocity gain zone. When n increases from 2 to 4, the maximum fragment velocity and average kinetic energy in the velocity gain zone increase by 186.7 m/s (9.6%) and 259.7 J (3.6%) respectively. When n increases from 4 to 6, these parameters exhibit a slight increase of 30.7 m/s (1.4%) and 281.4 J (3.7%) respectively. Fragment velocity and kinetic energy do not change significantly between n=6 and n=8, with maximum velocity differing by only 2.1% and average kinetic energy by 1.4%. Increasing n from 2 to 4 expands the velocity gain zone but reduces fragment density, thereby decreasing kinetic energy per unit area and reducing energy density by 47.3%. When n increases from 4 to 6, the increased average fragment kinetic energy and reduced dispersion angle concentrate kinetic energy on the target, increasing energy density by 11.9%. Conversely, increasing n from 6 to 8 further enlarges the velocity gain zone and reduces fragment density, decreasing energy density by 11.5%.

A comprehensive analysis was performed on parameter changes under different initiation modes—including the velocity gain zone, warhead dispersion angle, fragment velocity, and energy density. When the number of initiation points n increases from 2 to 4, fragment energy density decreases significantly. However, the velocity gain zone expands substantially, fragment velocity and kinetic energy increase markedly, and the dispersion angle reduces considerably. These changes collectively enhance the warhead's lethality against targets. Under the research conditions of the work, further increasing n to 6 and 8 yields limited improvements in relevant parameters. In engineering applications, such an increase significantly elevates structural complexity and reduces effective explosive weight. Therefore, subsequent research focuses primarily on four-point eccentric initiated warhead.

Table 6 Comparative data for four-point eccentric initiation and single-point central initiation

Initiation mode	Single-point central initiation	Four-point eccentric initiation	Gain
Maximum velocity (m/s)	1599.2	2138.3	33.7%
Average velocity (m/s)	1484.9	1846.7	24.3%
Average kinetic energy(j)	4894.6	7570.6	54.7%
Average specific kinetic energy(J/cm^2)	9412.7	14558.8	54.7%
Energy density (J/m^2)	50155.8	131484.1	162.2%
Dispersion angle/°	8.4	5.4	-35.7%

Statistical data for the warhead under single-point central initiation, including fragment velocity, kinetic energy, energy density at 12 m from the explosive center, and dispersion angle within the $\theta \in [138^{\circ}, 222^{\circ}]$ angular sector, were compared with those for four-point eccentric initiation. The corresponding performance gains are presented in Table 6. The data demonstrate that in contrast to central initiation, four-point eccentric initiation, within the velocity gain zone, exhibits maximum fragment velocity, average kinetic energy, and energy density increased by 33.7%, 54.7%, and 162.2% respectively, and dispersion angle reduced by 35.7%. These results confirm that four-point eccentric initiation significantly enhances the warhead’s strike efficacy relative to single-point central initiation.

4. Conclusions

To investigate the fragment dispersion characteristics of eccentrically initiated semi-preformed focused warheads by simulation, central initiation experiments were used to validate the feasibility of the simulation models. To analyze the effects of initiation conditions on warhead fragmentation and dispersion characteristics, detonation processes under different initiation conditions were simulated, revealing the influence of the number and axial positions of initiation points on fragment velocity, energy, and dispersion within the velocity gain zone.

As the number of axial initiation points increases, the velocity gain zone expands. In contrast, the warhead dispersion angle, average fragment velocity, and kinetic energy peak first and then decline, while the energy density initially decreases and then exhibits slight fluctuations. A comprehensive analysis confirms that, under the research conditions, four-point eccentric symmetrical initiation outperforms single-point central initiation, with maximum velocity within the velocity gain zone, average kinetic energy, and energy density increased by 33.7%, 54.7%, and 162.2% respectively, and dispersion angle reduced by 35.7%.

Based on the influence laws of initiation modes on fragment dispersion established in the work, combined with the effects of casing materials, fragmentation control methods, generatrix characteristics, the number of initiation points, and target position on fragmentation in focused warheads, the research provides a theoretical foundation for designing and analyzing fragmentation lethality in such warheads.

Acknowledgments

This research was partially supported by the National Natural Science Foundation of China (NSFC) (Grant No. 12472364).

References

[1] Fan C, Yao Y, Xue P, Zhang M, et al. Technics development situation of the low-cost precision guided ammunition. Tactical Missile Technology, 2020(01): 39-46, doi:10.16358/j.issn.1009-1300.2020.1.504.

[2] Liang A, Zheng X, Sun X. A fragment warhead technology on air defense missile. Journal of Projectiles, Rockets, Missiles and Guidance, 2021, 41(05): 86-90, doi:10.15892/j.cnki.djzdxb.2021.05.017.

[3] Sun X, Zhang G, Yang S. Study on fragments dispersing direction control of directional warhead. Journal of Projectiles, Rockets, Missiles and Guidance, 2008, 28(1): 102-104, doi:10.3969/j.issn.1673-9728.2008.01.030.

[4] Arnold W. Controlled fragmentation. AIP Conference Proceedings, 2002, 620(1): 527-530, doi:10.1063/1.1483593.

[5] Villano D, Galliccia F. Innovative technologies for controlled fragmentation warheads. Journal of Applied Mechanics, 2013, 80(3): 031704, doi:10.1115/1.4023341.

[6] Li Y, Xiong S, Li X, Wen Y. Mechanism of velocity enhancement of asymmetrically two lines initiated warhead. International Journal of Impact Engineering, 2018, 122: 161-174, doi:10.1016/j.ijimpeng.2018.07.011.

[7] Guo Z, Huang G, Chen P, Li X, et al. Fragments dispersion characteristics of the casing with the mismatched shell under internal explosive loading. International Journal of Impact Engineering, 2023, 171: 104370, doi:10.1016/j.ijimpeng.2022.104370.

[8] Chen H, Li S, Yang C. Modeling and simulation of the initiation control of the warhead by the hexagon-detection fuze. Modern Defence Technology, 2022, 50(05): 140-151, doi:10.3969/j.issn.1009-086x.2022.05.018.

[9] Rong J, Gan Z, Qin G, et al. Effect of initiation manners on scattering characteristics of double-beam focusing warhead. Journal of Beijing Institute of Technology, 2016, 36(04): 359-364+375, doi:10.15918/j.tbit1001-0645.2016.04.005.

[10] Johnson G, Cook W. A constitutive model and data for metals subjected to large strains, high strain rates and high temperatures. Engineering Fracture Mechanics, 1983, 21: 541-548.

[11] Baudin G, Serradeill R. Review of Jones-Wilkins-Lee equation of state. EPJ Web of Conferences, 2010, 10: 00021, doi:10.1051/epjconf/20101000021.

[12] Carlucci D, Jacobson S. Ballistics: theory and design of guns and ammunition, 2007, doi:10.1201/9781420066197.

[13] Zhang J, Sun H, Li C, Li B. Damage test research on typical fragments destroy concrete targets. Journal of Ordnance Equipment Engineering, 2022, 43(09): 309-314, doi:10.11809/bqzbgcxb2022.09.044.

[14] Wang L. Research on the dispersion characteristics of fragments from a cylindrical casing under eccentric initiation. Beijing Institute of Technology, 2017, doi:10.26948/d.cnki.gbjlu.2017.000025.